Optical properties of high-pressure fluid hydrogen across molecular dissociation

Giovanni Rillo[a], Miguel A. Morales[b], David M. Ceperley[c,1], and Carlo Pierleoni[d,e,1]

[a]Department of Physics, Sapienza University of Rome, 00185 Rome, Italy; [b]Physics Division, Lawrence Livermore National Laboratory, Livermore, CA 94550; [c]Department of Physics, University of Illinois Urbana–Champaign, Urbana, IL 61801; [d]Department of Physical and Chemical Sciences, University of L'Aquila, 67010 L'Aquila, Italy; and [e]Maison de la Simulation, CEA, CNRS, Univ. Paris-Sud, UVSQ, Université Paris-Saclay, 91191 Gif-sur-Yvette, France

Contributed by David M. Ceperley, March 12, 2019 (sent for review November 5, 2018; reviewed by Russell J. Hemley and Ronald Redmer)

Optical properties of compressed fluid hydrogen in the region where dissociation and metallization is observed are computed by ab initio methods and compared with recent experimental results. We confirm that at $T > 3{,}000$ K, both processes are continuous, while at $T < 1{,}500$ K, the first-order phase transition is accompanied by a discontinuity of the dc conductivity and the thermal conductivity, while both the reflectivity and absorption coefficient vary rapidly but continuously. Our results support the recent analysis of National Ignition Facility (NIF) experiments [Celliers PM, et al. (2018) *Science* 361:677–682], which assigned the inception of metallization to pressures where the reflectivity is ∼0.3. Our results also support the conclusion that the temperature plateau seen in laser-heated diamond-anvil cell (DAC) experiments at temperatures higher than 1,500 K corresponds to the onset of optical absorption, not to the phase transition.

hydrogen | high pressure | metal insulator | optical properties | quantum Monte Carlo

Metallization of hydrogen is a fundamental, yet elusive, process in the crystalline phase and controversial in the fluid phase. For example, it has been proposed (1) that solid hydrogen under compression will undergo a sequence of transitions from the insulating molecular phase becoming semiconducting and semimetallic before it enters the fully metallic atomic phase. Metallic fluid hydrogen has been unequivocally detected by Weir and coworkers (2, 3) at pressures of ~ 140 GPa and temperatures of 2,500–3,000 K using dynamical compression with shockwaves. The emergence of the metallic state was detected by a direct measure of sample resistivity, but they were unable to make a clear characterization of the insulator–metal (IM) transition (4).

Recent static-compression experiments, using a diamond-anvil cell (DAC) with controlled laser heating (short-pulses DAC; sp-DAC) (5–9), studied fluid hydrogen and deuterium, measuring both temperature and pressure. An absorber was heated with short laser pulses; the heat was transferred to the sample by thermal conduction. The sample temperature was observed to grow linearly with the power of the laser impulses until a plateau in the temperature was observed. The onset of the plateau was interpreted as the occurrence of a first-order phase transition (6).

Similar experiments at higher temperatures ($T > 2{,}000$ K) confirmed the observation (12). Optical measurements during laser heating observed an increase in reflectivity until saturation when $R \simeq 0.5$, at a temperature higher than the plateau (7–9) (Fig. 1).

During dynamic (ramp plus small shocks) compression experiments on deuterium using the Z-machine (17), the sample became first opaque and later, at higher pressure, had an abrupt change in reflectivity, suggesting a discontinuous IM transition. However, this transition occurred at a much higher pressure (∼150 GPa) than in the DAC experiments. The temperature was not directly measured; it was inferred by using a model equation of state (EOS). They found a temperature-independent transition line in contrast to the observation for hydrogen in the DAC experiments. Such a large difference cannot be ascribed to the isotopic effect. Previous shock-compression experiments on deuterium by Fortov et al. (18) found indirect evidence of a discontinuous transition much closer to those of Zaghoo et al. (7). Very recent experiments (19) with dynamic compression of deuterium at the National Ignition Facility (NIF) confirmed the Z-machine observation of a first regime of absorption followed by a rapid rise of reflectivity, again up to a plateau of ~ 0.5. However, this rise was observed at lower pressures, ∼100 GPa lower than at the Z-machine, closer to the results of static-compression experiments and in agreement with theoretical predictions from quantum Monte Carlo (QMC) methods (10, 20, 21). The metallization transition was assumed to occur when reflectivity at the D–LiF interface equaled 0.3. This corresponds to the minimum metallic conductivity of ∼2,000 S/cm (2, 3). In contrast to the Z-machine experiments, they did not observe hysteresis in the reflectivity during compression and decompression of the sample.

In a third experimental method, a microsecond-long laser impulse heats a DAC sample (lp-DAC) (13, 14). By using ultrafast spectroscopy, both the signature of high-temperature metallization and the emergence of the absorbing state during the cooling process were detected.

In Fig. 1, we show the emerging phase diagrams of hydrogen and deuterium from the various experiments. Also shown are the liquid–liquid phase transitions (LLPTs) for the two

Significance

The properties of warm, dense hydrogen are important in material science, plasma physics, planetary science, and astrophysics. We present simulations of its behavior in relation to ongoing, and in some cases controversial, results from static- and dynamic-compression experiments. The optical properties of dense liquid hydrogen are computed under conditions such that hydrogen is changing from a molecular insulating fluid into an atomic metallic fluid. The computed reflectivity and absorption of light agree with recent experimental observations and reconcile the observations with each other, leading to an understanding of this transition, thereby guiding future experimental and theoretical work, as well as being useful for planetary and astrophysical models.

Author contributions: M.A.M., D.M.C., and C.P. designed research; G.R., M.A.M., and C.P. performed research; M.A.M. and C.P. contributed new reagents/analytic tools; G.R., M.A.M., D.M.C., and C.P. analyzed data; and M.A.M., D.M.C., and C.P. wrote the paper.

Reviewers: R.J.H., The George Washington University; and R.R., Rostock University, Germany.

The authors declare no conflict of interest.

[1]To whom correspondence may be addressed. Email: ceperley@illinois.edu or carlo.pierleoni@aquila.infn.it.

This article contains supporting information online at www.pnas.org/lookup/suppl/doi:10.1073/pnas.1818897116/-/DCSupplemental.

Published online April 30, 2019.

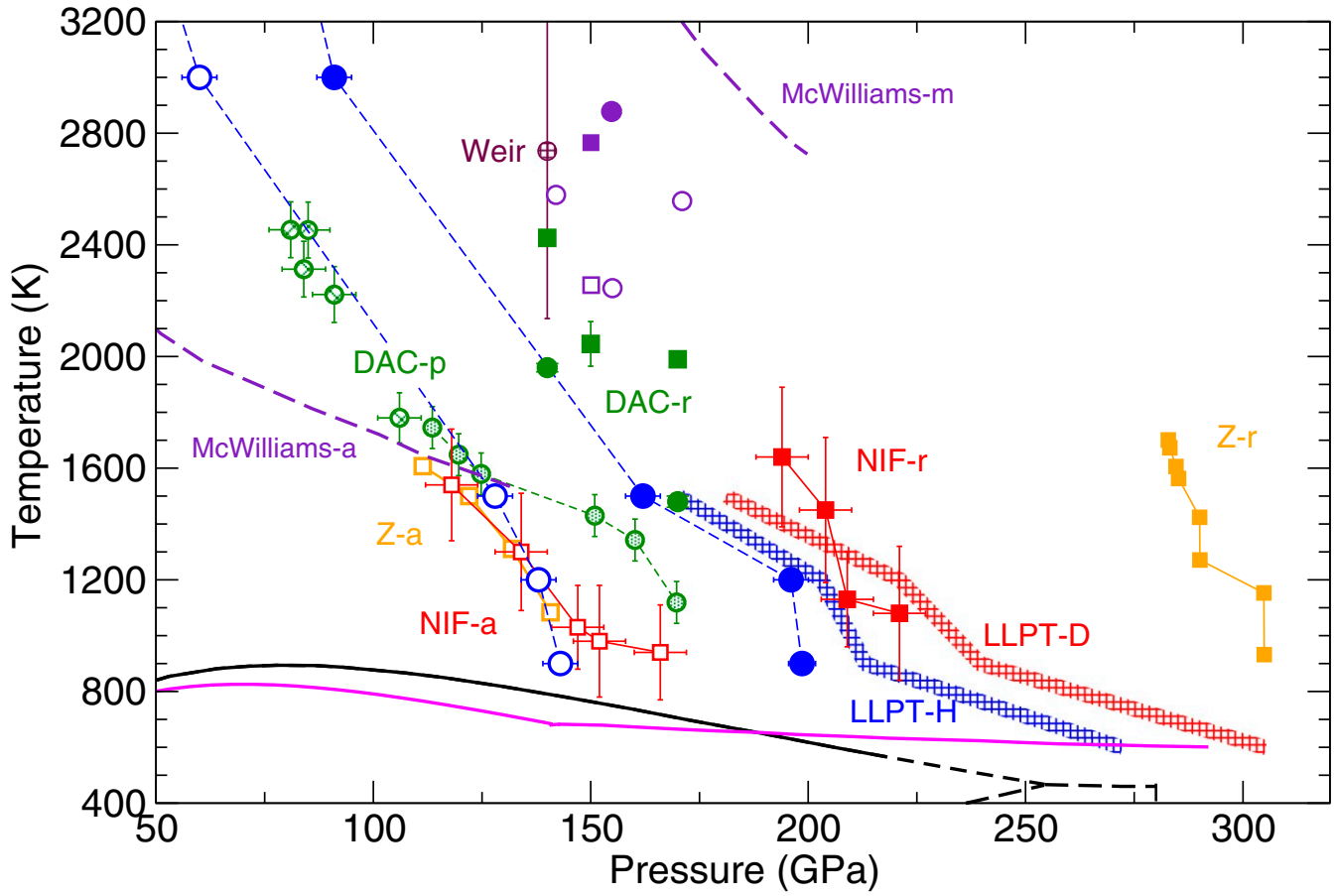

Fig. 1. Phase diagrams of hydrogen and deuterium around the LLPT line. Shaded lines (blue for hydrogen and red for deuterium) are the LLPT predicted by CEIMC (10, 11). Filled symbols are estimates of the LLPT from the reflectivity coefficient; open symbols indicate the inception of absorption. Squares correspond to deuterium, circles to hydrogen. Shown are data from sp-DAC (green), Z-machine (orange), NIF (red), and lp-DAC methods (purple). DAC-p, data from sp-DAC corresponding to the temperature plateau from refs. 6 and 7 ($T \leq 1{,}700$) and from ref. 12 ($T \geq 1{,}700$); DAC-r, data from sp-DAC at $R = 0.3$; lp-DAC (13), filled purple points are conducting conditions, and open purple points are nonconducting conditions (for both hydrogen and deuterium); NIF-a, data from NIF when the absorption coefficient $> 1\ \mu m^{-1}$; NIF-r, data from NIF at $R = 0.3$; Z-a, data from Z-machine when the sample becomes dark; Z-r, data from Z-machine at the observed discontinuity in reflectivity. Two dashed purple lines indicate the inception of absorption (McWilliams-a) and the metallic boundary (McWilliams-m) (14). Brown shaded circles (Weir) show the inception of metallicity from gas gun experiments (2). Blue points are theoretical estimates from this study: Filled circles show when $R = 0.3$ for H/vacuum interface; open circles shown when the absorption coefficient equals $1\ \mu m^{-1}$. Two slightly different melting lines are reported at low temperature (15, 16).

sotopes from coupled electron-ion Monte Carlo (CEIMC) calculations (10) as well as results obtained in this work from optical properties.*

Note that shock-compression experiments do not provide direct information about the molecular character of the sample, and it is very difficult to observe the weakly first-order character of the fluid–fluid transition (10, 11). The signal of the transition is obtained from optical measurements, mainly the reflectivity and absorption coefficients. Moreover, in shock experiments, the temperature is inferred from theoretical models which can lead to large uncertainties. In static-compression experiments, information about the molecular character can be inferred by vibrational spectroscopy and the temperature estimated from the optical emissivity. Spectroscopic identification of molecular character is difficult near the transition once the reflectivity increases, but a Drude model can be used to estimate the density of conduction electrons.

Theoretical predictions of hydrogen metallization and molecular dissociation have been provided by chemical models (22, 23), which suggested the existence of a first-order transition line, and by first-principles simulation methods (15). Results of early calculations (24–30) gave differing predictions. More recent and accurate investigations (10, 17, 20, 21, 31–36) indicated the presence, below a critical temperature, of a first-order transition between an insulating molecular fluid and a conducting monoatomic fluid. This picture emerges both from Born–Oppenheimer molecular dynamics (BOMD) using a variety of exchange-correlation approximations and from CEIMC (37). Hence, the existence of a first-order LLPT with a negative P–T slope is a robust prediction of theory. Nuclear quantum effects change the location of the phase transition by tens of gigapascals (10, 11, 17, 34) but preserve the first-order character. The location of the transition line, on the other hand, depends significantly on the details of the simulation. The results from QMC-based methods [CEIMC (10) and QMC-based molecular dynamics (21)], which are more reliable than BOMD, lie between the static-compression experiment predictions (7, 12)

*In reality, the system is in the fluid state since the critical point of the liquid–gas transition line is at much lower pressure and temperature. However, in the past literature, the term "liquid–liquid phase transition," and the corresponding acronym LLPT, has been widely used, and we prefer here to use it as well to avoid further confusion.

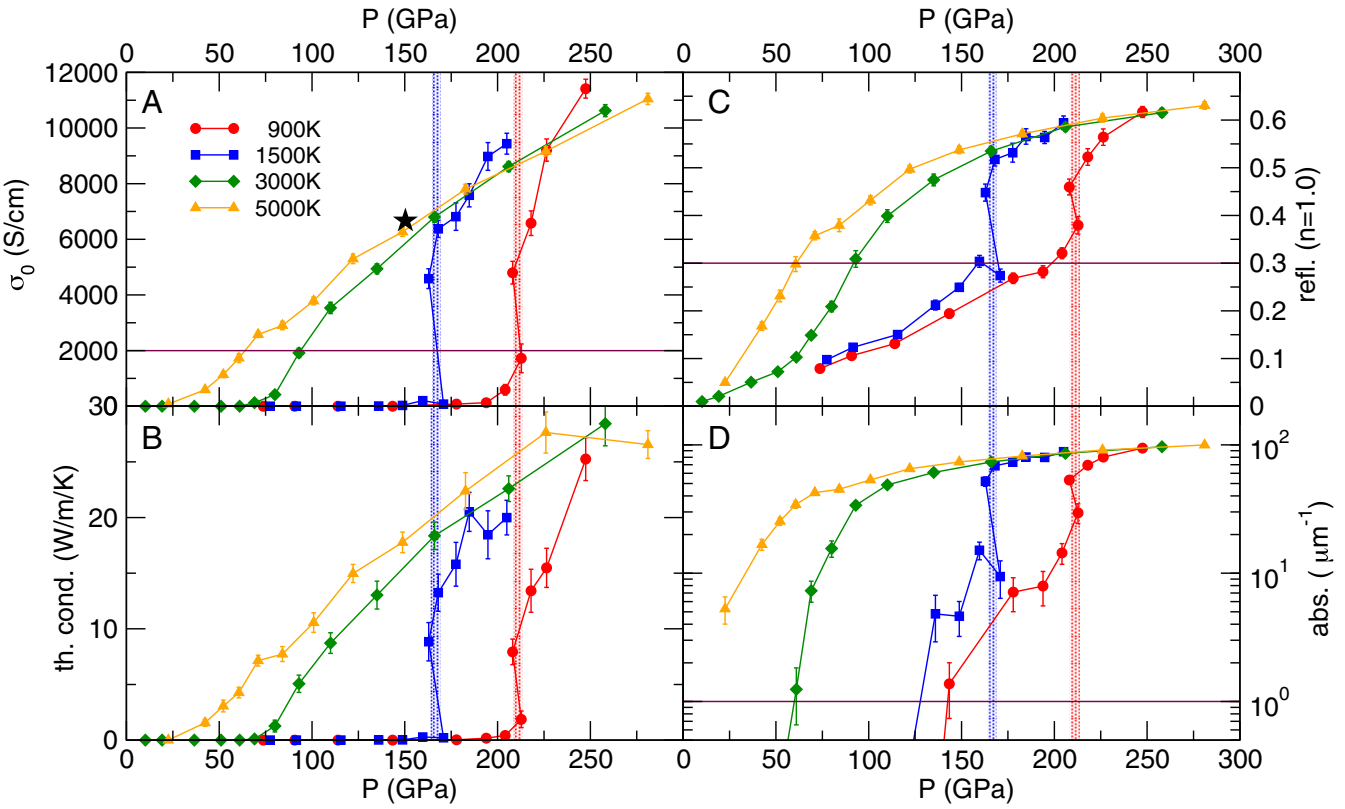

Fig. 2. Linear response properties of liquid hydrogen along the isotherms: T = 900 K, 1,500 K, 3,000 K, and 5,000 K. Configurations along the two lower isotherms were obtained by CEIMC, while configurations at 3,000 K and 5,000 K were obtained by PIMD. (*A*) Static electrical conductivity σ_0. The black star is a data point from ref. 13 for deuterium at 4,400 K. (*B*) Thermal conductivity (th. cond.). (*C*) Reflectivity (refl.) at $\omega = 2.3$ eV corresponding to an optical wavelength of $\lambda = 539$ nm, at a vacuum interface. (*D*) Absorption (abs.) coefficient at $\omega = 2.3$ eV. The vertical dashed lines indicate the pressure of the LLPT, as observed in the EOS (10, 11) for T = 900 K (red) and T = 1,500 K (blue). The horizontal line in *A* represents the minimum metallic conductivity of 2,000 S/cm, while in *C* and *D*, it corresponds to the threshold values used in interpreting the NIF experiments (19).

and the dynamic compression from the Z-machine (17) and were in excellent agreement with the recent NIF data (19).

Electronic properties across the transition region, such as optical conductivity and reflectivity, can be computed by the Kubo–Greenwood formula (38, 39) within density functional theory (DFT) (10, 20, 32–34).[†] By using nuclear configurations sampled by both BOMD and CEIMC, the static conductivity was found to be discontinuous at the transition. The molecular character of the fluid suddenly disappeared within CEIMC (10, 11); hence, the dissociation transition coincided with the IM transition. At the same time, a discontinuous behavior of the electronic momentum distribution was observed at the transition and was associated with a change of electronic localization from non-Fermi to Fermi liquid character (41). Within BOMD, the molecular character disappeared more slowly above the transition, but details depended on the specific functional used (17, 20, 36).

In this work, we used CEIMC and path-integral BOMD (PIMD) to perform simulations of high-pressure liquid hydrogen in the region of the molecular dissociation and metallization in a temperature range including both the first-order transition at low temperature and the cross-over at higher temperature. We then computed the optical properties with DFT [as was performed in the solid (1)], in particular, the reflectivity and the absorption coefficients, which are the key measured properties.[‡] We found that, even at temperatures below the critical point, where the dc conductivity had a discontinuity of ~ 4 orders of magnitude, the reflectivity at the experimental frequency showed only a rapid increase, in agreement with experimental observations, both at NIF and at the Z-machine (although the latter experiment reported higher pressure; SI Appendix, Fig. S2). In agreement with the experimental picture, we found a lower pressure for the sample to become absorbing (assigned to the pressure at which absorption equals $1\ \mu m^{-1}$) and a higher pressure for the reflectivity to exceed $R \simeq 0.3$. Moreover, we show that below the critical point, where the variation in reflectivity across the LLPT is more rapid, the value $R \simeq 0.3$ corresponds to a pressure value very close to the observed LLPT and, hence, to the transition to the metallic state. Above the critical point, this criterion ($R \simeq 0.3$) is more qualitative but still a rather good indication of the cross-over. We observed a substantial reflectivity even for "insulating" molecular hydrogen at conditions close to the transition line. Our calculations show that the rapid but continuous change of reflectivity observed in dynamic experiments (19) is consistent with a first-order fluid–fluid transition. Moreover, our calculations suggest that, for $T \geq$ 1,500 K, the temperature plateau observed in sp-DAC experiments (6, 7, 12) correspond to the inception of optical absorption, not to the phase transition, as suggested (17).

[†] A correlated-electron method [correlation function QMC method (40)] to compute electrical conductivity beyond the single-electron picture of Kubo–Greenwood has only been applied at temperatures higher than the critical point.

[‡] The experimental determination of conductivity has been achieved only in early gas gun experiments (2, 3).

CEIMC simulations of liquid hydrogen were performed at densities corresponding to pressures between 50 and 250 GPa along three isotherms: T = 900 K, 1,200 K, and 1,500 K. PIMD simulations were performed along the isotherms T = 3,000 K, 5,000 K, 6,000 K, and 8,000 K.

Our main results are reported in Fig. 2. The electrical and thermal conductivities are static values ($\omega = 0$); the reflectivity and the absorption coefficients were computed at $\omega = 2.3$ eV, corresponding to $\lambda = 539$ nm, a typical value used in experiments (9, 14, 17, 19). Fig. 2 *A* and *B* clearly show a discontinuity in the electrical and thermal conductivities at lower temperatures, indicating a first-order IM transition. The curves are smooth at higher temperatures ($T \geq$ 3,000 K), consistent with the termination of the first-order transition line at the estimated critical temperature (between 1,500 K and 3,000 K) (10, 11, 20). Above the critical temperature, molecular dissociation and metallization become a continuous "cross-over."

In contrast, the reflectivity and absorption coefficients, shown in Fig. 2 *C* and *D*, are not discontinuous, even below the critical point. Absorption coefficients $>1\,\mu m^{-1}$—the threshold value used in ref. 19 between transparent and opaque regime—happened between 50 and 150 GPa, depending on temperature. Those pressure values are shown in Fig. 1 as open blue circles. The pressure difference between this value and the critical pressure was ∼50 GPa. The absorption saturated at $\simeq 100\,\mu m^{-1}$ at higher pressures. The darkening of the sample with pressure was associated with the reduction of the energy gap to the energy of the laser's photons. Reflectivity also increased smoothly with pressure from zero up to a saturation value of ~ 0.6. For temperatures below the critical point, we observed an abrupt jump of $\sim 0.1 - 0.2$ in the reflectivity, in close correspondence to the LLPT transition (more visible at T = 1,500 K). However, the reflectivity at pressures just below the transition was already quite substantial ($R \sim 0.3$). The horizontal line in Fig. 2*C* represents the threshold value $R = 0.3$ used in ref. 19 to establish the minimum metallic conductivity of 2,000 S/cm, used to estimate the IM transition. The pressures when $R = 0.3$ at various temperatures are shown in Fig. 1 as filled blue circles. Comparing Fig. 2 *A* and *C*, we see that $R = 0.3$ matches well with the pressures where the conductivity reaches 2,000 S/cm, confirming the experimental analysis.[§] Below the critical temperature, the value $R = 0.3$ is very close to the observed reflectivity on the low pressure side of the LLPT.

The reflectivity in Fig. 2*C* was computed, assuming a reflecting interface with air ($n = 1.0$). However, in experiments, different materials were used. At NIF, a LiF window was used with a refractive index of $n \sim 1.5$ at the relevant pressures. Fig. 3 shows the reflectivity obtained with a material of refractive index $n = 1.49$ and compares with the data in Fig. 2*C*. We saw a rigid downward shift of the reflectivity along all isotherms; the saturation value at high pressures dropped from ~ 0.6 to ~ 0.5. Below the critical point, due to the vertical jump of reflectivity at the transition, the pressure corresponding to R = 0.3 was slightly increased, improving the agreement with the LLPT pressure, which confirms the validity of the criterion used to interpret the NIF experiments. However, above the critical temperature, changing the refractive index of the contrasting medium substantially changed the pressure corresponding to $R = 0.3$. While for $n = 1$, $R = 0.3$ and σ_0 = 2,000 S/cm corresponded to the same pressures, for $n = 1.49$, the two pressures differed: 20 GPa at 3,000 K and 35 GPa at 5,000 K. We note that this criterion is only qualitative. Increasing the refractive index of the window material will require higher pressures to reach R = 0.3, corresponding to larger values of the conductivity.

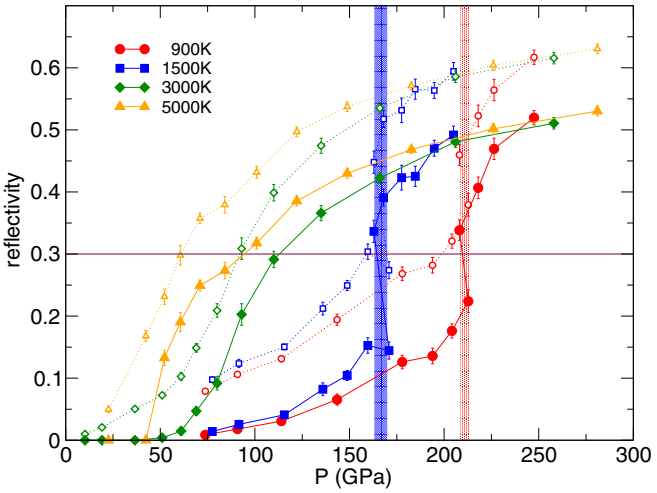

Fig. 3. Dependence of the reflectivity of liquid hydrogen along isotherms for differing window materials. Filled symbols correspond to a material with $n = 1.49$ (LiF) and open symbols to a material with $n = 1.0$ (vacuum). Colors and symbols, as well as vertical dashed and horizontal continuous lines, are as described in Fig. 2.

Fig. 1 shows the estimated hydrogen and deuterium phase diagrams in the region of the fluid–fluid transition both from experiments and theory. There are two main sets of data points aligned along diagonal descending lines. The line at lower pressure is where the absorption coefficient reaches the threshold of $1\,\mu m^{-1}$, according to NIF data and to our present results (from Fig. 2*D*). Data points from the observed temperature plateaus in sp-DAC experiments followed the same behavior for $T >$ 1,500 K. At lower temperatures, they moved to slightly higher pressure. The second diagonal line is where the reflectivity reaches the value $R = 0.3$ in NIF experiments and in our calculations with $n = 1.0$. Note that NIF data are for deuterium, while our results are for hydrogen, so we do not expect perfect agreement. We also report the LLPT transition line from ref. 10. As noted above, the value $R = 0.3$ was reached slightly before the transition point. Data at $n = 1.49$ would be in better agreement with the transition pressures below the critical temperature, and the high temperature point will move toward higher pressure by ∼20–30 GPa (and even more for windows with a larger refractive index). The reflectivity data from static-compression experiments lie along the same line both for hydrogen (8) and deuterium (9).[¶]

We performed simulations of high-pressure liquid hydrogen in the region of molecular dissociation and metallization, using state-of-the-art first-principles methods [CEIMC and vdW-DF-PIMD)]. We computed optical properties in the Kubo–Greenwood framework and compared them with existing experimental data. Our work confirmed the validity of the proposed analysis of NIF data, in particular that a rapid but continuous increase of reflectivity is still compatible with the existence of a weakly first-order LLPT found in first-principles simulations (10). Moreover, we confirm that below the critical temperature, the transition pressure can be associated with a reflectivity value of $R \simeq 0.3$, which also corresponds to the sudden jump in conductivity of ∼4 orders of magnitude. Above the critical point, where the dissociation–metallization process is continuous, a reflectivity of R = 0.3 corresponds to

[§]A similar analysis is reported in the supplementary material of ref. 17 (see figure S7).

[¶]The same criterion of $R = 0.3$ has been used to extract these data.

conductivity values >2,000 S/cm, with the precise value depending on the refractive index of the window material.

Materials and Methods

CEIMC calculations were performed with our research code BOPIMC. Systems with 54 and 128 hydrogen atoms were studied, in the pressure range of 50–250 GPa. A detailed description of the CEIMC simulation parameters, along with an assessment of their accuracy, is given in the supporting information of ref. 10. PIMD simulations were performed with a modified version of VASP (42). The vdW-DF1 exchange-correlation functional was used in PIMD simulations. We performed calculations both at the gamma point and with a $3 \times 3 \times 3$ Monkhorst–Pack grid of k points to study the sensitivity of the metallization process. A time-step of 8 $(\text{a.u.})^{-1}$ was used in all PIMD simulations. Finite-temperature electronic effects were taken into account by using Fermi–Dirac smearing. For the calculation of optical properties, we used linear-response theory based on the Kubo–Greenwood formulation. The HSE functional, with 25% of exact exchange (43), was used to calculate all of the optical properties reported in this work. Sixteen uncorrelated nuclear configurations from the trajectory were sampled at each density and temperature. These were then used to calculate the optical conductivity, reflectivity, absorption coefficient, and electronic thermal conductivity. Statistical averages and error analysis were performed by using the results of the 16 nuclear configurations. Static ($\omega = 0$) values of the conductivities were obtained by extrapolating finite energies ($\omega > 0$) data using a standard procedure (20, 33). Technical details are reported in ref. 44.

ACKNOWLEDGMENTS. We thank P. Loubeyre, R. Redmer, and P. Celliers for useful discussions. We thank I. Silvera and M. Zaghoo for details of their experimental analysis. M.A.M. was supported by the US Department of Energy (DOE), Office of Science, Basic Energy Sciences, Materials Sciences and Engineering Division, as part of the Computational Materials Sciences Program and Center for Predictive Simulation of Functional Materials. This work was performed in part under the auspices of the US DOE by Lawrence Livermore National Laboratory under Contract DE-AC52-07NA27344. D.M.C. was supported by DOE Grant NA DE-NA0002911 and by the Fondation NanoSciences (Grenoble). C.P. was supported by the Agence Nationale de la Recherche France, under the program "Accueil de Chercheurs de Haut Niveau 2015" Project HyLight-Extreme. Computer time was provided by Partnership for Advanced Computing in Europe (PRACE) Project 2016143296, by an allocation of the Blue Waters sustained petascale computing project, supported by National Science Foundation Award OCI 07- 25070 and the State of Illinois, and by the high-performance computer resources from Grand Equipement National de Calcul Intensif (GENCI) Allocation 2018-A0030910282.

1. Cohen RE, Naumov II, Hemley RJ (2013) Electronic excitations and metallization of dense solid hydrogen. *Proc Natl Acad Sci USA* 110:13757–13762.
2. Weir ST, Mitchell AC, Nellis WJ (1996) Metallization of fluid molecular hydrogen at 140 GPa (1.4 Mbar). *Phys Rev Lett* 76:1860–1863.
3. Nellis WJ, Weir ST, Mitchell AC (1999) Minimum metallic conductivity of fluid hydrogen at 140 GPa (1.4 Mbar). *Phys Rev B* 59:3434–3449.
4. Nellis W, Louis A, Ashcroft N (1998) Metallization of fluid hydrogen [and discussion]. *Philos Trans Math Phys Eng Sci* 356:119–138.
5. Silvera I, Deemyad S (2009) Pathways to metallic hydrogen. *Low Temp Phys* 35: 318–325.
6. Dzyabura V, Zaghoo M, Silvera IF (2013) Evidence of a liquid–liquid phase transition in hot dense hydrogen. *Proc Natl Acad Sci USA* 110:8040–8044.
7. Zaghoo M, Salamat A, Silvera IF (2016) Evidence of a first-order phase transition to metallic hydrogen. *Phys Rev B* 93:155128.
8. Zaghoo M, Silvera IF (2017) Conductivity and dissociation in liquid metallic hydrogen and implications for planetary interiors. *Proc Natl Acad Sci USA* 114:11873–11877.
9. Zaghoo M, Husband RJ, Silvera IF (2018) Striking isotope effect on the metallization phase lines of liquid hydrogen and deuterium. *Phys Rev B* 98:104102.
10. Pierleoni C, Morales MA, Rillo G, Holzmann M, Ceperley DM (2016) Liquid–liquid phase transition in hydrogen by coupled electron–ion Monte Carlo simulations. *Proc Natl Acad Sci USA* 113:4954–4957.
11. Pierleoni C, Holzmann M, Ceperley DM (2017) Local structure in dense hydrogen at the liquid-liquid phase transition by coupled electron-ion Monte Carlo. *Contrib Plasma Phys* 58:99–106.
12. Ohta K, et al. (2015) Phase boundary of hot dense fluid hydrogen. *Sci Rep* 5:16560.
13. Jiang S, et al. (2018) Insulator-metal transition in liquid hydrogen and deuterium. arXiv:1810.01360. Preprint, posted October 2, 2018.
14. McWilliams RS, Allen Dalton D, Mahmood MF, Goncharov AF (2016) Optical properties of fluid hydrogen at the transition to a conducting state. *Phys Rev Lett* 116: 255501.
15. McMahon JM, Morales MA, Pierleoni C, Ceperley DM (2012) The properties of hydrogen and helium under extreme conditions. *Rev Mod Phys* 84:1607–1653.
16. Zha C-S, Liu H, Tse JS, Hemley RJ (2017) Melting and high P-T transitions of hydrogen up to 300 GPa. *Phys Rev Lett* 119:075302.
17. Knudson MD, et al. (2015) Direct observation of an abrupt insulator-to-metal transition in dense liquid deuterium. *Science* 348:1455–1460.
18. Fortov VE, et al. (2007) Phase transition in a strongly nonideal deuterium plasma generated by quasi-isentropical compression at megabar pressures. *Phys Rev Lett* 99:185001.
19. Celliers PM, et al. (2018) Insulator-metal transition in dense fluid deuterium. *Science* 361:677–682.
20. Morales MA, Pierleoni C, Schwegler E, Ceperley DM (2010) Evidence for a first-order liquid-liquid transition in high-pressure hydrogen from ab initio simulations. *Proc Natl Acad Sci USA* 107:12799–12803.
21. Mazzola G, Helled R, Sorella S (2018) Phase diagram of hydrogen and a hydrogen-helium mixture at planetary conditions by quantum Monte Carlo simulations. *Phys Rev Lett* 120:025701.
22. Ebeling W, Richert W (1985) Plasma phase transition in hydrogen. *Phys Lett A* 108: 80–82.
23. Saumon D, Chabrier G (1989) Fluid hydrogen at high density: The plasma phase transition. *Phys Rev Lett* 62:2397–2400.
24. Magro WR, Ceperley DM, Pierleoni C, Bernu B (1996) Molecular dissociation in hot, dense hydrogen. *Phys Rev Lett* 76:1240–1243.
25. Scandolo S (2003) Liquid–liquid phase transition in compressed hydrogen from first-principles simulations. *Proc Natl Acad Sci USA* 100:3051–3053.
26. Bonev S, Schwegler E, Ogitsu T, Galli G (2004) A quantum fluid of metallic hydrogen suggested by first-principles calculations. *Nature* 431:669–672.
27. Delaney KT, Pierleoni C, Ceperley DM (2006) Quantum Monte Carlo simulation of the high-pressure molecular-atomic crossover in fluid hydrogen. *Phys Rev Lett* 97:235702.
28. Vorberger J, Tamblyn I, Militzer B, Bonev SA (2007) Hydrogen-helium mixtures in the interiors of giant planets. *Phys Rev B* 75:024206.
29. Vorberger J, Tamblyn I, Bonev SA, Militzer B (2007) Properties of dense fluid hydrogen and helium in giant gas planets. *Contrib Plasma Phys* 47:375–380.
30. Holst B, Redmer R, Desjarlais MP (2008) Thermophysical properties of warm dense hydrogen using quantum molecular dynamics simulations. *Phys Rev B* 77:184201.
31. Liberatore E, Morales MA, Ceperley DM, Pierleoni C (2011) Free energy methods in coupled electron ion Monte Carlo. *Mol Phys* 109:3029–3036.
32. Lorenzen W, Holst B, Redmer R (2010) First-order liquid-liquid phase transition in dense hydrogen. *Phys Rev B* 82:195107.
33. Holst B, French M, Redmer R (2011) Electronic transport coefficients from ab initio simulations and application to dense liquid hydrogen. *Phys Rev B* 83:235120.
34. Morales MA, McMahon JM, Pierleoni C, Ceperley DM (2013) Nuclear quantum effects and nonlocal exchange-correlation functionals applied to liquid hydrogen at high pressure. *Phys Rev Lett* 110:065702.
35. Norman DE, Saitov IM (2017) Critical point and mechanism of the fluid–fluid phase transition in warm dense hydrogen. *Dokl Phys* 62:294–298.
36. Gorelov V, Pierleoni C, Ceperley DM (February 17, 2019) Benchmarking vdW-DF first principle predictions against coupled electron-ion Monte Carlo for high pressure liquid hydrogen. *Contrib Plasma Phys*, 10.1002/ctpp.201800185.
37. Pierleoni C, Ceperley DM (2006) The coupled electron-ion Monte Carlo method. *Lecture Notes in Physics* (Springer, Berlin), Vol 703, pp 641–683.
38. Kubo R (1957) Statistical-mechanical theory of irreversible processes. I. General theory and simple applications to magnetic and conduction problems. *J Phys Soc Jpn* 12: 570–586.
39. Greenwood DA (1958) The Boltzmann equation in the theory of electrical conduction in metals. *Proc Phys Soc* 71:585–596.
40. Lin F, et al. (2009) Electrical conductivity of high-pressure liquid hydrogen by quantum Monte Carlo methods. *Phys Rev Lett* 103:256401.
41. Pierleoni C, Rillo G, Ceperley DM, Holzmann M (2018) Electron localization properties in high pressure hydrogen at the liquid-liquid phase transition by coupled electron-ion Monte Carlo. *J Phys Conf Ser* 1136:012005.
42. Kresse G, Furthmüller J (1996) Efficiency of ab-initio total energy calculations for metals and semiconductors using a plane-wave basis set. *Comput Mater Sci* 6:15–50.
43. Heyd J, Peralta JE, Scuseria GE, Martin RL (2005) Energy band gaps and lattice parameters evaluated with the Heyd-Scuseria-Ernzerhof screened hybrid functional. *J Chem Phys* 123:174101.
44. Rillo G (2016) A quantum Monte Carlo study of high pressure solid and liquid hydrogen. PhD thesis (University of Rome "La Sapienza," Rome).

Supporting Information for: Optical properties of high pressure fluid hydrogen across molecular dissociation

Giovanni Rillo[a], **Miguel A. Morales**[b], **David M. Ceperley**[c], **and Carlo Pierleoni**[d,e]

[a]Department of Physics, Sapienza University of Rome, P.le A. Moro,2, 00185 Rome, Italy; [b]Physics Division, Lawrence Livermore National Laboratory, Livermore, CA USA; [c]Department of Physics, University of Illinois Urbana-Champaign, Urbana, IL, 61821 USA; [d]Department of Physical and Chemical Sciences, University of L'Aquila, Via Vetoio 10, 67010 L'Aquila, Italy; [e]Maison de la Simulation, CEA, CNRS, Univ. Paris-Sud, UVSQ, Université Paris-Saclay, 91191 Gif-sur-Yvette, France

This manuscript was compiled on April 17, 2019

In figures 1 and 2 we compare our results for the conductivity and the reflectivity of hydrogen to the corresponding results for deuterium obtained by first-principles molecular dynamics using the vdW-DF2 XC approximation (1) within DFT. In both properties we observe a pressure shift between our present results for hydrogen and the results for deuterium in ref. (1). Moreover, this pressure shift, measured as the difference between the D and H pressures at $\sigma_0 = 2000 S/cm$ at the same temperature, is sensitive to the temperature: it is $\sim 50 GPa$ at 3000K and $\sim 150 GPa$ at 1500K. There are two different effects to account for the origin of this difference: the different treatment of the electronic exchange and correlation and the different treatment of nuclear quantum effects. Our calculation assumes quantum protons and we have sampled the nuclear configurations with the electronic energy determined by VMC energies through the CEIMC method along the isotherms at T=900K and 1500K and by first-principles Path Integral MD (PIMD) with the vdW-DF functional along the isotherms at 3000K and 5000K. In contrast, the simulations reported in ref. (1) considered classical protons and sampled the configuration space with FPMD using the vdW-DF2 functional. In the past we have observed that vdW-DF2 predicts a transition pressure larger than CEIMC by about 100GPa(2) while the vdW-DF and CEIMC derived transition pressures are rather close to each other(3, 4). Moreover, nuclear quantum effects are known to reduce the transition pressure by $\sim 20 - 60 GPa$ depending on temperature. The two effects together account for the pressure shift observed.

Another potential source of the difference is the DFT functional employed to perform the optical calculations. Our optical calculations employ the HSE functional. In ref. (1) the vdW-DF2 has been used for the optical calculations and then a reduction of both conductivity and reflectivity with respect to HSE is expected (2). Despite these differences the qualitative behavior of our and Knudson's results are quite similar. In particular, both sets of data show a saturation of reflectivity ~ 0.5 (with a LiF window assuming $n_0 = 1.49$) and both have a tendency toward a common, temperature independent, behavior of the conductivity at high pressure.

Next we compare our calculated conductivity with the experimental determination by Nellis, Weir and Mitchell (6). The experimental set up allowed a direct measure of pressure and resistivity, while the temperature and density were inferred using a model EOS. A recent work reconsidered those data and established the accuracy of various DFT functionals to reproduce the experimental measurements(7). In figure 3 we report the experimental conductivity for both hydrogen and deuterium together with our results for hydrogen. First

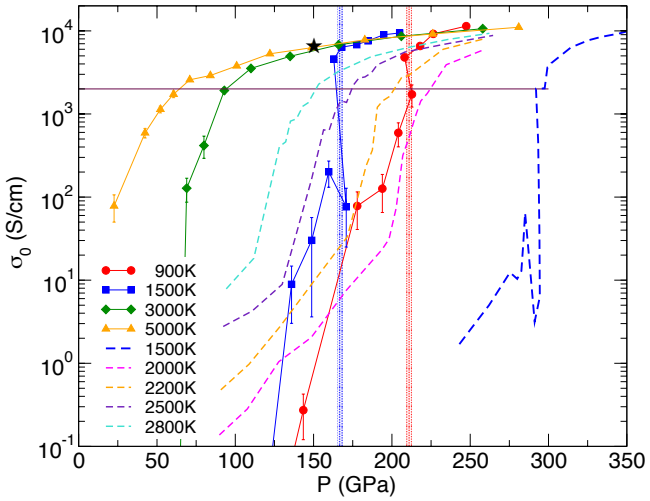

Fig. 1. DC conductivity for hydrogen (continuous lines and symbols) from this work and deuterium (dashed lines) from ref (1). The black star is a data point from ref. (5) for deuterium at 4400K.

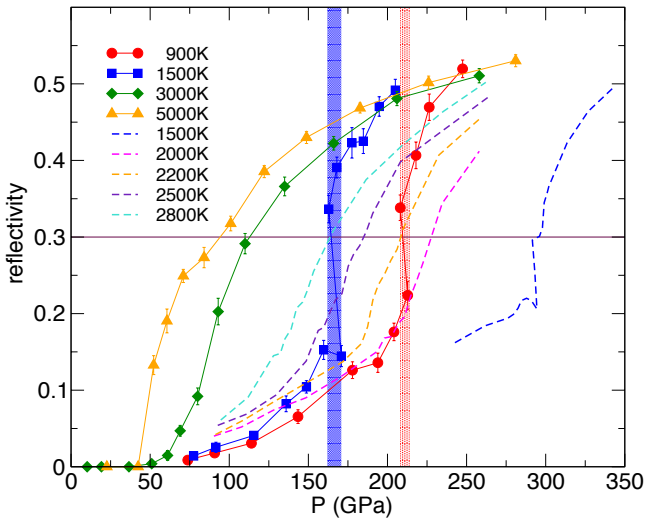

Fig. 2. Reflectivity for hydrogen at $\omega = 2.3eV$ (continuous lines and symbols) from this work and for deuterium at $532nm = 2.33eV$ (dashed lines) from ref. (1). In both calculation a window of LiF with $n_0 = 1.49$ was assumed.

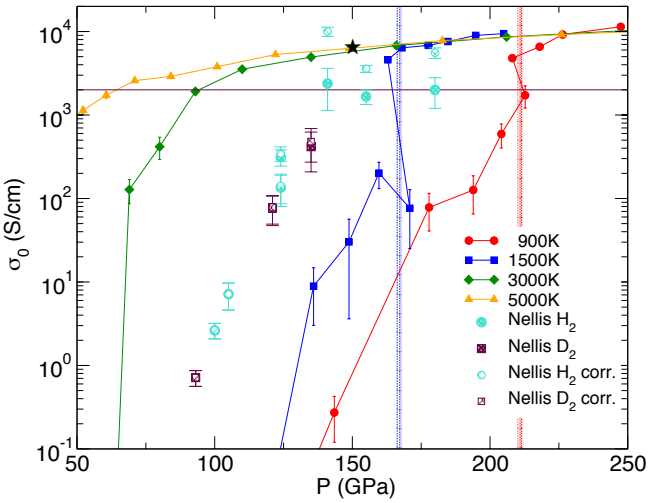

Fig. 3. Comparison of our conductivity predictions for hydrogen with experimental data from ref (6) for both hydrogen (light blue solid circles) and deuterium (brown solid squares). Experimental data corrected as discussed in the text are represented by open circles for hydrogen and open squares for deuterium.

we notice that experimental data for hydrogen and deuterium align along a common line. The temperature in these experiments is unknown but our comparison suggests that they are all at about the same temperature, intermediate between 1500K and 3000K. Secondly we note that the experimental data seems to saturate around $\sigma_0 = 2000 S/cm$ a value rather smaller than the saturation predicted both by CEIMC and FPMD with different functionals (see figure 1). A possible way to reconcile experiments and theories would be to imagine the presence of a, pressure independent, resistive bias in series with the sample during the measurement. In this situation the sample conductivity would be

$$\sigma_0(P) = \frac{\sigma_{exp}(P)}{1 - \rho_s \sigma_{exp}(P)} \qquad [1]$$

where $\sigma_{exp}(P) = 1/\rho_{exp}(P)$ and ρ_{exp} is the measured value for the resistivity and ρ_s is the resistivity of the biasing element. Assuming a value of $\rho_s = 3.2 \times 10^{-4} \Omega cm$, eq. (1) provides the results represented by open symbols in fig.3 which are in a better agreement with the theoretical predictions. Note that the effect of this bias would be negligible until the saturation is reached, while it significantly affects results around saturation. But whether this kind of mechanism could be invoked remains to be established.

1. Knudson MD, et al. (2015) Direct observation of an abrupt insulator-to-metal transition in dense liquid deuterium. *Science* 348(6242):1455–1460.
2. Morales MA, McMahon JM, Pierleoni C, Ceperley DM (2013) Nuclear quantum effects and nonlocal exchange-correlation functionals applied to liquid hydrogen at high pressure. *Phys. Rev. Letts.* 110(6):065702.
3. Pierleoni C, Morales MA, Rillo G, Holzmann M, Ceperley DM (2016) Liquid–liquid phase transition in hydrogen by coupled electron–ion Monte Carlo simulations. *Proc. Natl. Acad. Sci.* 113(18):4954–4957.
4. Gorelov V, Pierleoni C, Ceperley DM (2019) Benchmarking vdw-df first principle predictions against coupled electron-ion monte carlo for high pressure liquid hydrogen. *Contribution to Plasma Physics* e201800185:https://doi.org/10.1002/ctpp.201800185.
5. Jiang S, et al. (2018) Insulator-metal transition in liquid hydrogen and deuterium, arxiv:1810.01360.
6. Nellis WJ, Weir ST, Mitchell AC (1999) Minimum metallic conductivity of fluid hydrogen at 140 GPa (1.4 Mbar). *Phys. Rev. B* 59(5):3434–3449.
7. Knudson MD, Desjarlais MP, Preising M, Redmer R (2018) Evaluation of exchange-correlation functionals with multiple-shock conductivity measurements in hydrogen and deuterium at the molecular-to-atomic transition. *Phys. Rev. B* 98:174110.